In Situ Dielectric Characterization of Poly(ethylene oxide) Melts Containing Lithium Perchlorate under Steady Shear Flow

Yumi Matsumiya,[†,‡,§] Nitash P. Balsara,[*,†,‡,∥] John B. Kerr,[∥] Tadashi Inoue,[§] and Hiroshi Watanabe[*,§]

Department of Chemical Engineering, University of California, and Environmental Energies and Technologies Division and Materials Sciences Division, Lawrence Berkeley National Laboratory, Berkeley, California 94720, and Institute for Chemical Research, Kyoto University, Uji, Kyoto 611-0011, Japan

Received August 27, 2003; Revised Manuscript Received November 4, 2003

ABSTRACT: For poly(ethylene oxide) (PEO) melts containing lithium perchlorate ($LiClO_4$), angular frequency ω dependence of the dynamic dielectric properties under steady shear flow was measured using a rheodielectric instrument. The instrument also enabled measurements of the dielectric properties in the quiescent state as well as the linear and nonlinear rheological properties. A significant increase in the zero-shear viscosity η_0 was observed upon addition of $LiClO_4$ to PEO, and this increase was attributed to Li^+-mediated intermolecular bridging of the PEO chains formed in the quiescent state. Significant shear thinning of the steady-state viscosity $\eta(\dot{\gamma})$ was observed with increasing shear rate $\dot{\gamma}$, suggesting the flow-induced breakup of these bridges. The presence of liberated ions was detected directly by dielectric experiments under steady shear flow. The dielectric dispersion (due to the electrode polarization of the ions) shifted to higher ω with increasing $\dot{\gamma}$, indicating an increase in the ionic conductivity σ. The dispersion curves for different $\dot{\gamma}$ values collapsed onto a single master curve when plotted against a reduced frequency, $\{\lambda(\dot{\gamma})\}^{-1}\omega$, where $\lambda(\dot{\gamma})$ was a $\dot{\gamma}$-dependent shift factor representing the increase of σ. This result strongly suggested that the increase of σ under shear flow was due to an increase in the ionic mobility μ by the factor of $\lambda(\dot{\gamma})$ and not due to a change in the number density of ions. Furthermore, excellent agreement was found between the $\eta(\dot{\gamma})/\eta_0$ ratio and $\{\lambda(\dot{\gamma})\}^{-1}$. This agreement reflected a strong motional cooperativivity between the PEO chain segment and ion (Li^+).

1. Introduction

There is continuing interest in obtaining a fundamental understanding of the physical properties of ion-containing polymeric systems. These materials have the potential of affecting a wide range of applications from batteries to fuel cells.[1−23] The performance of polymer electrolytes in the battery applications depends on three parameters: electrical conductivity, the fraction of charge transported by the cation (transference number), and salt diffusivity. Despite considerable efforts,[1−23] many fundamental questions regarding the mechanism of charge transport in these systems remain unresolved.

A common example of polymer electrolytes is a polar polymer such as poly(ethylene oxide) (PEO) with a salt such as lithium perchlorate ($LiClO_4$) mixed in. The miscibility between the salt and polymer is usually due to attractive interactions between the polymer and the ions. Experimental manifestations of these interactions include an increase in the glass transition temperature T_g upon addition of the salt and nonmonotonic dependence of the electrical conductivity σ on the salt concentration.[1,5,7,13−15,20,21] Molecular dynamics simulations, indicating that dissociated Li^+ ions are surrounded by a cage comprising three to six contiguous ethylene oxide monomers,[17] are consistent with this experimental observation.

For mixtures containing monovalent salts, σ is expressed as

$$\sigma = e(\mu_+ + \mu_-)n \tag{1}$$

where μ_+ and μ_- are the mobilities of the cation and anion, respectively, n is the number density of the dissociated cation (identical to that of the dissociated anion), and e is the absolute value of the charge of an electron. Obtaining polymer electrolytes with high electrical conductivity can be thus achieved by increasing either the number density n or the mobility μ of the ions.

To understand the factors that affect the electrical conductivity of polymer electrolytes, it is important to determine n and μ independently. Experimental methods for accomplishing this include the inversion current method,[8] radioactive tracer method,[9] NMR,[10] infrared/Raman spectroscopy,[11,12] and dielectric dispersion.[14,15,20−23] These experiments suggest that the ions are more or less bound to neighboring polymer segments. The motion of ions and polymer segments is thus cooperative, and the ionic mobility μ decreases with increasing n. The increase of T_g with increasing salt concentration is a natural consequence of this retardation of segmental motion, and the nonmonotonic dependence of σ on the salt concentration reflects a competition between the increase of n and the resulting decrease of μ.

While the validity of the qualitative relationships between the mechanical and electrical properties of polymer electrolytes described above has been confirmed, frameworks that quantitatively predict these relationships have not been established. The difficulty stems from the coupled nature of the mobilities of the segments and ions.

* To whom correspondence should be addressed.
† University of California.
‡ Environmental Energies and Technologies Division, Lawrence Berkeley National Laboratory.
§ Kyoto University.
∥ Materials Sciences Division, Lawrence Berkeley National Laboratory.

10.1021/ma0304473 CCC: $27.50
Published on Web 12/23/2003

In this paper we demonstrate that an in situ measurement of the dynamic dielectric properties of polymer electrolytes under steady shear flow enables the decoupling of these effects. Our experiments were conducted on PEO melts containing $LiClO_4$, using a specially designed rheodielectric instrument. The instrument also enabled measurements of the dielectric properties in the quiescent state as well as the linear and nonlinear rheological properties. In the quiescent state, the system exhibited pronounced dielectric dispersion at low angular frequencies ω attributable to the electrode polarization of the ions, as well-known for similar systems.[1,14,15,22,23] Under fast shear, the dispersion shifted to higher ω, indicating an increase in the electrical conductivity σ, while the steady-state viscosity η exhibited strong nonlinear shear thinning. Analysis of the dielectric data indicated that the shear-induced increase of σ was due entirely to an increase in the ion mobility; the dissociation constant of the polymer electrolyte was unaffected by the shear flow. Furthermore, the shear-induced increase in the ion mobility was well correlated to the shear thinning of the viscosity. Details of these results are presented below.

2. Experimental Section

PEO samples with weight-averaged molecular weights $10^{-3}M = 1$, 10, and 20 and polydispersity index $M_w/M_n \cong 2$, designated as PEO-1K, PEO-10K, and PEO-20K, and $LiClO_4$ were purchased from Aldrich. These materials were used as received. Polymer/salt mixtures were made by dissolving predetermined masses of PEO and $LiClO_4$ in excess methanol, followed by complete removal of methanol, first at atmospheric temperature and pressure followed by drying in a vacuum oven at 60 °C for 1 week. The $LiClO_4$ concentration in all of the mixtures studied was 2.3 kmol m^{-3}, corresponding to a Li:ethylene oxide molar ratio of 1:10.

The systems described above were subjected to dielectric and rheological measurements. The neat PEO samples were also studied for comparison. The dynamic dielectric constant ϵ' and dielectric loss ϵ'' were measured as a function of angular frequency ω in the quiescent state and under steady shear with automated capacitance bridges (SI 1260 impedance/gain-phase analyzer and 1296 dielectric interface, Solartron; GR1689, General Radio): ϵ' and ϵ'' are defined as the properties relative to the vacuum having the dielectric permittivity (static dielectric constant) $\epsilon_{vac} = 8.854 \times 10^{-12}$ F m^{-1}.[24]

The samples were placed between stainless steel, guarded cone-and-plate-type electrodes mounted on a laboratory rheometer (ARES, Rheometrics). The electrodes are shown schematically in Figure 1. The cone (main electrode) had radius $r_0 = 13.6$ mm and a gap angle $\theta = 0.058$ rad. The head of the cone was flattened over an area of radius $r_c = 3.6$ mm to avoid an electrical contact between the cone and plate electrodes. The cone electrode was supported by an insulating block made of a machinable ceramic and Teflon and mounted on the guard electrode of outer radius $r = 15.0$ mm. The plate electrode (counter electrode) also had $r = 15.0$ mm. During steady shear, the electrical contact between the impedance analyzer and the rotating electrode (cone electrode) was made through a stainless steel contact ring dipped into a mercury reservoir; see Figure 1. This reservoir enabled good electrical contact without mechanical disturbances due to rapid rotation of the electrode.[25−31]

The frequency-dependent storage and loss moduli in the linear viscoelastic limit, G' and G'', and the shear-rate-dependent steady-state viscosity η of the samples under steady shear flow were measured using the cone-and-plate rheodielectric cell on the rheometer explained above. The range of strains over which linear response was obtained was determined before the linear viscoelastic measurements were conducted.

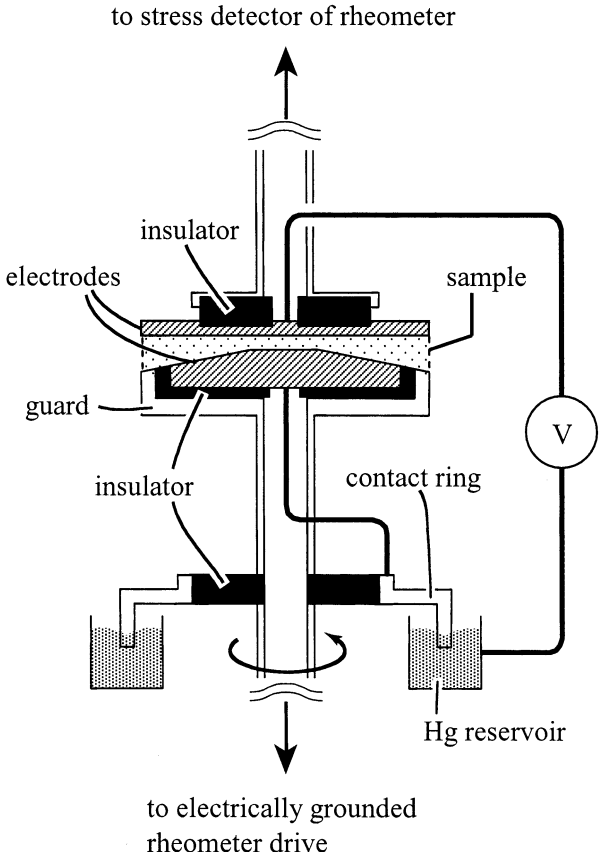

Figure 1. Schematic illustration of the rheodielectric setup.

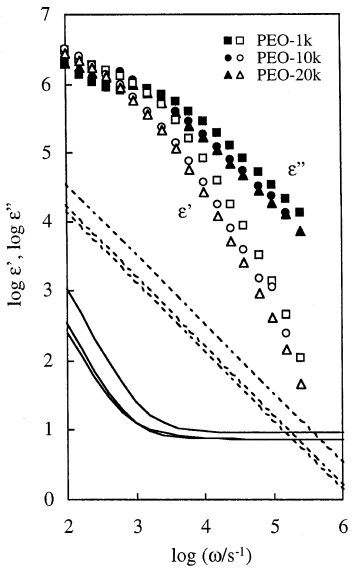

Figure 2. Dielectric behavior of PEO/$LiClO_4$ systems with a salt concentration of 2.3 kmol m^{-3} at 60 °C. Unfilled and filled symbols denote dynamic dielectric constant ϵ' and dielectric loss ϵ'', respectively. For comparison, ϵ' and ϵ'' of neat PEO samples are shown with solid and dotted curves: PEO-1K, PEO-10K, and PEO-20K for the curves from top to bottom.

3. Results and Discussion

3.1. Dielectric Behavior in the Quiescent State. For the PEO/$LiClO_4$ mixtures, Figures 2 and 3, respectively, show the dielectric data measured at 60 and 25 °C in the quiescent state (symbols). The PEO-1K/$LiClO_4$ mixture melted at 15 °C, and the PEO-10K/$LiClO_4$ and PEO-20K/$LiClO_4$ mixtures melted at 50 °C. These

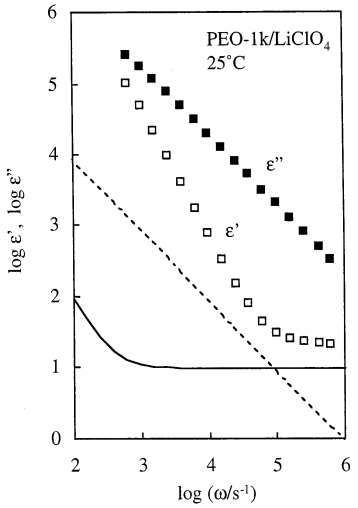

Figure 3. Dielectric behavior of the PEO-1K/$LiClO_4$ system with a salt concentration of 2.3 kmol m^{-3} at 25 °C. Unfilled and filled squares denote dynamic dielectric constant ϵ' and dielectric loss ϵ'', respectively. For comparison, ϵ' and ϵ'' of the neat PEO-1K sample are shown with solid and dotted curves.

mixtures were amorphous liquids at the temperatures examined in Figures 2 and 3.

The data for the PEO/$LiClO_4$ mixtures are to be compared with the data for the amorphous liquids of neat PEO at the *same* temperatures. However, neat PEO-1K melted at 40 °C and neat PEO-10K and PEO-20K melted at 67 °C so that the data in their amorphous liquid state could not be directly measured at the temperatures examined in Figures 2 and 3, 60 and 25 °C (except for the neat PEO-1K at 60 °C). For this reason, we measured the dielectric ϵ' and ϵ'' data of the neat PEO samples at several temperatures above their melting temperatures T_m. These data exhibited Arrhenius behavior and were accurately extrapolated to 60 and/or 25 °C.[32] (The extrapolation was not needed for the data of neat PEO-1K at 60 °C.)

In Figures 2 and 3, the extrapolated data of neat PEO are shown with the curves. These data, representing the behavior of neat PEO in the (supercooled) amorphous liquid state at the temperatures examined in Figures 2 and 3, can be directly compared with the data of the PEO/salt mixtures. The PEO/salt mixtures melted at lower temperatures, as explained earlier. Thus, the mixed salt decreased T_m of PEO, which is indicative of a strong interaction between the PEO segments and salt.

Now, we turn our attention to the angular frequency ω dependence of ϵ' and ϵ'' data of PEO/salt mixtures. The PEO/$LiClO_4$ mixtures exhibit significant dielectric dispersion characterized by the increases of ϵ' and ϵ'' with decreasing ω (symbols in Figures 2 and 3). This dispersion is similar to that reported for other mixtures of salts and polar polymers[1,14,15,22,23] and can be attributed to the electrode polarization[34] of the dissociated ions in the PEO matrix. The neat PEO systems have much smaller ϵ' and ϵ'' and exhibit only weak dispersion (curves in Figures 2 and 3). This weak dispersion is attributable to the electrode polarization of ionic impurities remaining in the polymers (not due to the dielectric relaxation of PEO segments).

Here, a brief comment is needed for the electrode polarization. (For details, see a summary of the Macdonald theory[34] for this polarization given in Appendix A.) The electrode polarization occurs because of inefficient discharging of the ions at the electrodes. Under the oscillatory electric field, a standing wave is formed in the ion concentration profile and the ions tend to be concentrated near the electrodes at low ω. This leads to an enhanced storage of electric energy and a corresponding increase in ϵ' *at low* ω. The ions also increase the electrical conductivity, thereby enhancing the high-ω dielectric loss ϵ'' compared to ϵ'' of the neat medium, but this enhancement becomes less significant (and ϵ'' exhibits a dispersion peak) at low ω, where the increase in ϵ' due to the electrode polarization is saturated. It should also be noted that ϵ' and ϵ'' at such low ω depend on the gap width L between the electrodes and are not the simple material properties independent of the measurement geometry. (L determines the standing wavelength thereby affecting ϵ' and ϵ''.) This L dependence, resulting in a decrease of the dispersion frequency with increasing L, has been experimentally confirmed for polar polymer/salt mixtures[14,15] including our PEO/$LiClO_4$ mixtures.[35] However, in the remaining part of this paper, we focus on the dielectric behavior under a fixed alignment of the electrodes (constant L) and make no further discussion of the L dependence.

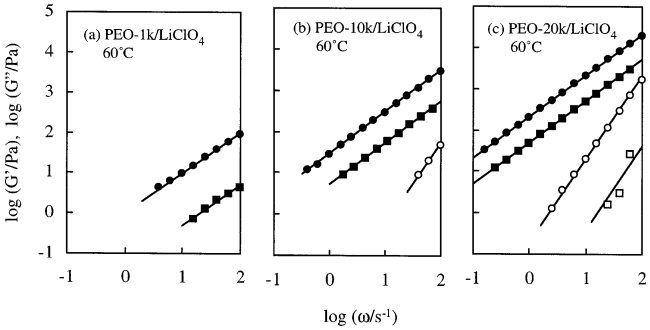

Figure 4. Storage and loss moduli G' and G'' (shown with unfilled and filled circles, respectively) obtained for PEO/$LiClO_4$ systems with a salt concentration of 2.3 kmol m^{-3} at 60 °C. For comparison, G' and G'' of neat PEO samples are shown with unfilled and filled squares, respectively.

At high frequencies ($\omega > 10^3$ s^{-1}), the ions in the PEO/$LiClO_4$ mixtures move without being affected by the electrodes so that their ϵ'' data are independent of L and proportional to ω^{-1} (symbols in Figures 2 and 3). In this range of ω, ϵ'' is the material property and related to the ω-independent electrical conductivity σ as

$$\sigma = \epsilon_{vac}\epsilon''\omega \tag{2}$$

where ϵ_{vac} is the dielectric permittivity of vacuum. The large increase in ϵ'' at high ω upon the addition of salt, seen in Figures 2 and 3, clearly indicates that some of the salt is in the dissociated state in the PEO matrix to increase σ.

3.2. Linear Viscoelastic Behavior. Figures 4 and 5 show the ω dependence of G' and G'' of our PEO/$LiClO_4$ mixtures measured at 60 and 25 °C, respectively (circles). The mixtures were amorphous liquids at these temperatures. The viscoelastic data for the amorphous liquids of neat PEO are needed for comparison, but the neat PEO samples were crystalline solids at those temperatures (except for the neat PEO-1K at 60 °C). Thus, G' and G'' of the neat PEO samples were measured at several temperatures above their melting temperatures T_m, as done for the dielectric data. These G' and G'' data of neat PEO exhibited Arrhenius

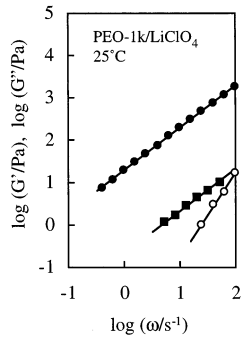

Figure 5. Storage and loss moduli G' and G'' (unfilled and filled circles) of the PEO-1K/$LiClO_4$ system with a salt concentration of 2.3 kmol m^{-3} at 25 °C. For comparison, G'' of the neat PEO-1K sample is shown with filled squares.

behavior and were accurately extrapolated to 60 and/or 25 °C.[32] The extrapolated data, representing the viscoelastic behavior of neat PEO in the (supercooled) amorphous liquid state at these temperatures, are shown with squares.

In all PEO systems, the G'' data exhibit the terminal behavior ($G'' \propto \omega$) over the accessible frequency window. For the PEO-1K system with and without salt at 60 °C (Figure 4a), G' was not well detected because the viscous dissipation dominated the viscoelastic response. However, for the PEO-1K/$LiClO_4$ system at 25 °C (Figure 5) and PEO-10K/$LiClO_4$ and PEO-20K/$LiClO_4$ systems at 60 °C (Figure 4b,c), an elastic response was clearly resolved to give G'. These G' data exhibit the terminal behavior ($G' \propto \omega^2$).

As clearly noted in Figures 4 and 5, G'' and the zero-shear viscosity η_0 ($=[G''/\omega]_{\omega\to 0}$) of the PEO/$LiClO_4$ systems are sigificantly larger than those of the neat PEO liquids at the same T (evaluated after the extrapolation from the melted regime). This can be attributed to two effects: **(1)** a retardation of segmental motion or, equivalently, an increase in T_g, and **(2)** the binding of multiple polymer chain segments to the Li^+ cation. Concerning the second effect, we note that the dielectric data (ϵ' and ϵ'') of the PEO/$LiClO_4$ systems are only weakly dependent on the PEO molecular weight M (Figure 2) while the viscoelastic behavior reflecting the large-scale motion of the chain drastically changes with M (Figure 4). This fact suggests the direct motional cooperativity between the ions and the chain segments,[7,14,15] not between the ions and the whole contour of the chain.

The steady-state compliance J_e^0 ($=[G'/\{G''\}^2]_{\omega\to 0}$) is a measure of the width of the distribution of the terminal viscoelastic relaxation modes.[33,36] The data shown in Figure 4c give $10^6 J_e^0/\mathrm{Pa}^{-1} = 4.9$ and 1.7 for PEO-20K with and without salt at 60 °C. Namely, J_e^0 is larger for the PEO-20K/salt system than for neat PEO-20K.

For the neat PEO-10K and PEO-1K samples, G' was too small to be detected so that J_e^0 cannot be determined experimentally. However, J_e^0 of these neat PEOs can be estimated on the basis of the Rouse relationship,[33,36] $J_e^0 \propto M$, valid for amorphous polymeric liquids having molecular weights $M \le M_c'$ (characteristic molecular weight for the compliance) and the same molecular weight distribution. M_c' is typically 4−5 times larger than the characteristic molecular weight M_c for the onset entanglement effect for viscosity,[33] and M_c of PEO is 4.4×10^3.[33] As judged from the corresponding M_c' value ($\cong 20 \times 10^3$), the neat PEO-20K, PEO-10K, and PEO-1K samples have $M \le M_c'$, and we may utilize the

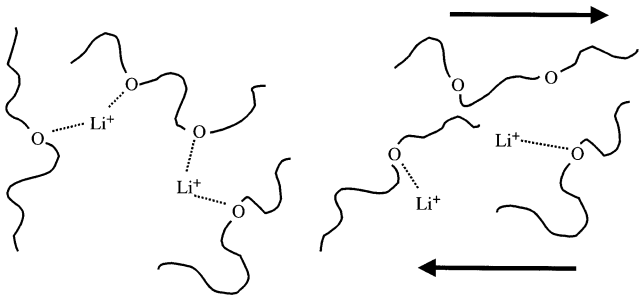

Figure 6. Schematic illustration of (a) dynamic aggregates of PEO chains bridged through Li^+ at equilibrium and (b) disruption of the aggregates under fast shear. The dotted lines indicate binding of Li^+ and oxygen in the PEO segment.

J_e^0 data (1.7×10^{-6} Pa^{-1}) of neat PEO-20K to obtain the estimates: $10^6 J_e^0/\mathrm{Pa}^{-1} \cong 1$ and 0.1 for the neat PEO-10K and neat PEO-1K, respectively. The J_e^0 data of the PEO-10K/salt and PEO-1K/salt mixtures determined from the G' and G'' data in Figures 4b and 5, $10^6 J_e^0/\mathrm{Pa}^{-1} = 4.4$ and 4.6, respectively, are significantly larger than these estimates (in particular for PEO-1K).

The above results indicate that J_e^0 of PEO increases upon the addition of salt. Since J_e^0 is quite sensitive to chain topology (e.g., branching) and insensitive to T_g,[33,36] this increase in J_e^0 can be exclusively attributed to the second effect explained above, namely, the binding of polymer chains by the Li^+ cations to create branched aggregates of the chains: The branch points are not permanent due to the mobility of Li^+. Since these branch points will occur randomly throughout the system, one expects to find considerable structural distribution in the polymer/salt mixtures, e.g., distributions in the branch length and number. This distribution should be responsible for the observed increase in J_e^0.

These dynamic aggregates, formed in the quiescent state at equilibrium, are illustrated schematically in Figure 6a. The Li^+ cation has a tendency to form a bridge between polar groups, as suggested by simulations[17] and known for carbanion/Li systems.[37] We now study the effect of steady shear flow on these aggregates. It is reasonable to expect that the Li^+-mediated aggregates will be disrupted under sufficiently fast shear, as illustrated in Figure 6b. This expectation is examined through dielectric and rheological tests under shear, as described below.

3.3. Dielectric and Non-Newtonian Flow Behavior under Steady Shear. The application of fast shear on high-M homopolymer melts results in shear thinning due to large distortion of polymer chains away from their equilibrium configurations.[33,36] The application of shear on our polymer/salt mixtures can, in principle, lead to disruption of either the Li^+-mediated aggregates or the distortion of the PEO chain configurations. To distinguish these possibilities, rheological and dielectric experiments under steady shear were conducted on the polymer/salt mixtures. The results are summarized below.

For PEO-1K/$LiClO_4$ and PEO-10K/$LiClO_4$ systems at 25 and 60 °C, respectively, Figure 7 shows changes of the viscosity growth function[33,36] $\eta^+(t;\dot\gamma)$ (transient shear stress after start-up of flow divided by the shear rate $\dot\gamma$) with time t after start-up of flow. The horizontal dotted lines indicate the zero-shear viscosity η_0 evaluated from the linear viscoelastic G'' data. For both

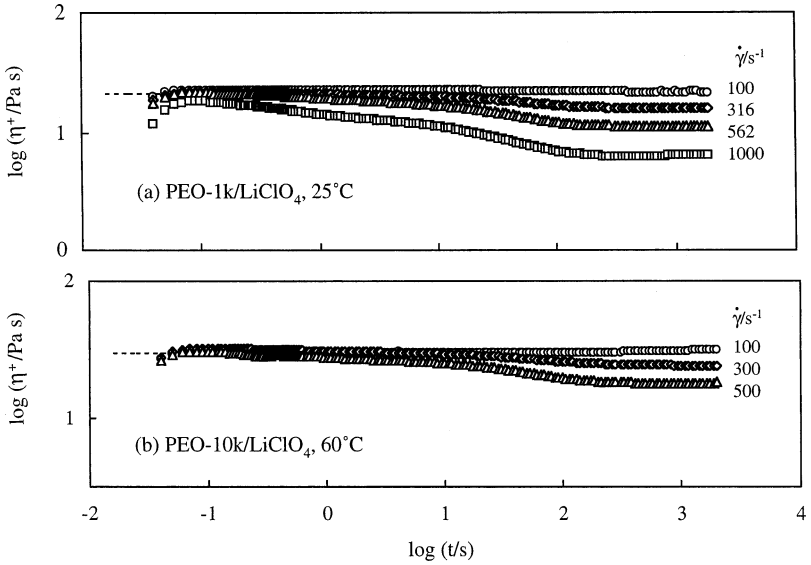

Figure 7. Viscosity growth function after start-up of steady shear measured for (a) the PEO-1K/$LiClO_4$ system at 25 °C and (b) the PEO-10K/$LiClO_4$ system at 60 °C. The horizontal dotted lines indicate the zero-shear viscosity η_0.

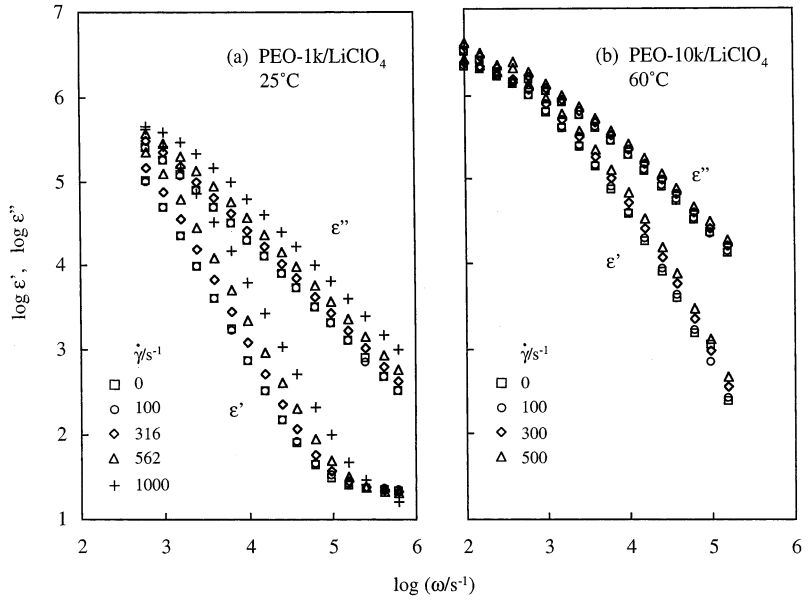

Figure 8. Dynamic dielectric constant ϵ' and dielectric loss ϵ'' under steady shear measured for (a) the PEO-1K/$LiClO_4$ system at 25 °C and (b) the PEO-10K/$LiClO_4$ system at 60 °C. For comparison, the ϵ' and ϵ'' data in the quiescent equilibrium state ($\dot{\gamma} = 0$) are also shown.

systems, $\eta^+(t;\dot{\gamma})$ increases to η_0 rapidly (within $t = 0.2$ s) irrespective of the shear rate $\dot{\gamma}$. Under slow shear at $\dot{\gamma} = 100\ s^{-1}$, $\eta^+(t;\dot{\gamma})$ remains constant ($\eta^+ = \eta_0$) at longer t and the steady zero-shear flow behavior is observed. In contrast, at $\dot{\gamma} \geq 300\ s^{-1}$, $\eta^+(t;\dot{\gamma})$ gradually decays with t and the steady flow associated with the non-Newtonian viscosity $\eta(\dot{\gamma}) = \eta^+(\infty;\dot{\gamma}) < \eta_0$ is achieved only at very long $t \geq 200$ s. The magnitudes of this shear thinning ($\eta(\dot{\gamma})/\eta_0 \cong 0.5$ at $\dot{\gamma} \cong 500\ s^{-1}$) are similar for the PEO-1K/$LiClO_4$ and PEO-10K/$LiClO_4$ systems.[38] At $\dot{\gamma} \leq 1000\ s^{-1}$ (the range of $\dot{\gamma}$ examined for the PEO/salt systems), no thinning was detected within the experimental accuracy for the neat PEO-1K and PEO-10K at temperatures just above their melting temperature. Thus, the gradual shear thinning of the PEO/salt systems is attributable to a flow-induced structural change, as discussed below.

In the linear viscoelastic regime, η_0 is much larger for the PEO/salt mixtures than for neat PEO (Figures 4 and 5). This increase of η_0 upon the addition of salt was attributed to two coupled effects, the aggregation of PEO chains mediated by Li^+ and the resulting decrease in the mobility of PEO segments. The decrease of η^+ (from η_0) seen in the nonlinear regime under the fast shear (Figure 7) would then be due to the disruption of the Li^+-mediated aggregates.[39] The η^+ data strongly suggest that the extent of the aggregate disruption, observed as the magnitude of shear thinning, increases with increasing shear rate. This observation lends support to the schematic depicted in Figure 6b.

If the Li^+ ions are liberated by steady shear, this must result in an increase in the electrical conductivity. Dielectric experiments under steady shear were conducted to test this hypothesis. The results are shown in parts a and b of Figure 8 for the PEO-1K/$LiClO_4$ system at 25 °C and the PEO-10K/$LiClO_4$ system at 60 °C, respectively. The $\epsilon'(\omega)$ and $\epsilon''(\omega)$ data obtained at a given angular frequency ω after the steady shear was

commenced changed during the first 100 s and then reached steady state. The data in Figure 8 were obtained in this steady state. The data obtained under the steady shear at $\dot{\gamma} = 100\ s^{-1}$ (circles) are indistinguishable from the data in the quiescent state (squares). However, the application of faster shear clearly results in increases in $\epsilon'(\omega)$ and $\epsilon''(\omega)$. Applying eq 2 to $\epsilon''(\omega)$ at $\omega > 10^3\ s^{-1}$ (where ϵ'' is proportional to ω^{-1}), we can conclude that the application of fast shear leads to an increase in the electrical conductivity in both systems. These dielectric features also support the schematic illustrated in Figure 6b.

All of the flow-induced changes in the rheological and dielectric properties of the polymer/salt mixtures were reversible; i.e., cessation of the flow for a few minutes resulted in the recovery of $G'(\omega)$, $G''(\omega)$, $\epsilon'(\omega)$, and $\epsilon''(\omega)$ to their equilibrium values. Interestingly, this recovery time (being required for re-formation of the Li^+-mediated aggregates of PEO) is comparable in magnitude with the time (≅200 s; Figure 7) necessary to disrupt the aggregates and achieve the steadily flowing state under fast shear.

3.4. Analysis of Rheological Data. The PEO-1K/$LiClO_4$ system at 25 °C and the PEO-10K/$LiClO_4$ system at 60 °C exhibit the terminal linear viscoelastic relaxation tails ($G' \propto \omega^2$ and $G'' \propto \omega$) in our experimental window; see Figures 4b and 5. From these tails, the terminal viscoelastic relaxation time $\langle\tau_G\rangle$ is evaluated as[33,36]

$$\langle\tau_G\rangle \cong \left[\frac{G'}{\omega G''}\right]_{\omega\to 0} = \begin{cases} 2 \times 10^{-4}\text{s} & \text{for PEO-10k/LiClO}_4\text{ at 60°C} \\ 8 \times 10^{-5}\text{s} & \text{for PEO-1k/LiClO}_4\text{ at 25°C} \end{cases} \quad (3)$$

This $\langle\tau_G\rangle$ can be assigned as the relaxation time of the Li^+-mediated aggregates in their nondisrupted form. The corresponding relaxation frequency of the nondisrupted aggregates, $\langle\omega_G\rangle = 1/\langle\tau_G\rangle$, is on the order of $10^4\ s^{-1}$.

In simple high-M homopolymer liquids, the shear rate at which deviations from the Newtonian behavior are observed is nearly equal to $\langle\omega_G\rangle$ and the time scale for the steady state to be achieved is less than $10\langle\tau_G\rangle$.[36] The behavior of our PEO/salt mixtures is considerably different. As noted in Figure 7, the shear thinning of the PEO-10K/$LiClO_4$ and PEO-1K/$LiClO_4$ systems is observed at shear rates $\dot{\gamma}$ considerably smaller than $\langle\omega_G\rangle$ ($=O(10^4)\ s^{-1}$). In addition, the steady-state value of η^+ is attained after 10^2 s, which is 5 orders of magnitude larger than $10\langle\tau_G\rangle$. It is natural that the disruption of the Li^+-mediated aggregates occurs gradually over a long interval of time (as observed) because the stress ($=\dot{\gamma}\eta^+$) causing the disruption decreases as the disruption proceeds with t.

Concerning this disruption, we note that the viscosities of the PEO/salt systems under fast shear are considerably larger than those of the corresponding neat PEO systems; $\eta = 6.8$ Pa s for PEO-1K/$LiClO_4$ at $\dot{\gamma} = 1000\ s^{-1}$ and $\eta_0 = 0.21$ Pa s for neat PEO-1K (both at 25 °C; cf. Figures 5 and 7a), and $\eta = 18$ Pa s for PEO-10K/$LiClO_4$ at $\dot{\gamma} = 500\ s^{-1}$ and $\eta_0 = 5.4$ Pa s for neat PEO-10K (both at 60 °C; cf. Figures 4b and 7b). This fact suggests that the Li^+-mediated aggregates were not disrupted into individual PEO chains (i.e., some aggregation remained) even under the fastest shear examined.

3.5. Analysis of Dielectric Data under Shear. We now analyze the dielectric data obtained under steady shear using the Macdonald theory for the electrode polarization of ions.[34] Some details of this theory are given in Appendix A. As explained there, the dispersion of ϵ' and ϵ'' in the parallel-plate geometry is determined by the mobilities of the cation and anion μ_+ and μ_-, the number density of cations/anions n, the gap width L between the electrodes, and the absolute temperature T. The theory indicates that the increases of μ and n result in different changes in the dispersion curves. For simplicity, we assume that the cations and anions have the same mobility μ. As shown in Appendix A, changes in μ alone result is a horizontal displacement of the log ϵ' versus log ω and log ϵ'' versus log ω curves. In addition, the displacements of both $\epsilon'(\omega)$ and $\epsilon''(\omega)$ curves along the abscissa (log ω) axis are the same and equal to the fractional change in μ (e.g., a factor of 10 increase in μ shifts the $\epsilon'(\omega)$ and $\epsilon''(\omega)$ curves to the high-ω side by 1 decade). This implies that a simple horizontal shift of the $\epsilon'(\omega)$ and $\epsilon''(\omega)$ data on double logarithmic plots will result in a superposed master curve. In contrast, changes in n result in changes in the $\epsilon'(\omega)$ and $\epsilon''(\omega)$ data along both the abscissa and ordinate. In this case a shift of the $\epsilon'(\omega)$ and $\epsilon''(\omega)$ data does not result in a single master curve (see Appendix A). This difference in the dielectric behavior in response to changes in μ and n, similar in the parallel-plate and cone-and-plate geometries (Appendix B), arises in theory because an increase in μ results in an increase in the dispersion frequency only, while an increase in n leads to increases of both dispersion frequency and intensity. The validity or failure of the superposition of the $\epsilon'(\omega)$ and $\epsilon''(\omega)$ data thus indicates the reason for the flow-induced increase in the electric conductivity σ ($=2e\mu n$ for the case of $\mu_+ = \mu_-$).

The $\epsilon'(\omega)$ and $\epsilon''(\omega)$ data given in Figure 8 were horizontally shifted to test the validity of the superposition explained above. The results are shown in parts a and b, respectively, of Figure 9. The same shift factor was used for the $\epsilon'(\omega)$ and $\epsilon''(\omega)$ data at a given shear rate, and the data obtained in the quiescent state ($\dot{\gamma} = 0$) were used as the reference for the shift. The magnitude of the horizontal shift for each set of data was chosen to obtain the best master curve; this procedure is similar to the procedure used to conduct the time−temperature superposition of linear viscoelastic data.[33]

For both PEO-1K/$LiClO_4$ at 25 °C and PEO-10K/$LiClO_4$ at 60 °C, Figure 9 demonstrates the excellent superposition of the dielectric data under steady shear at various rates. The shift factor λ at each shear rate gives the flow-induced increase in the average mobility of the ions μ. In Figure 10, the reciprocal shift factor λ^{-1} (circles) is plotted against a reduced shear rate, $\dot{\gamma}\langle\tau_G\rangle$, for convenience of comparison with the nonlinear thinning of the viscosity explained later. As seen in Figure 10, the average ion mobility increases by a factor of $\lambda = 3.2$ for PEO-1K/$LiClO_4$ at 25 °C and $\lambda = 1.5$ for PEO-10K/$LiClO_4$ at 60 °C in the range of the shear rate examined.

We have also conducted a quantitative comparison of our dielectric dispersion data and Macdonald theory under a simplifying assumption of equal mobility of the ions. For our cone−plate-type electrodes, the change in the gap width L with the distance r from the cone−plate

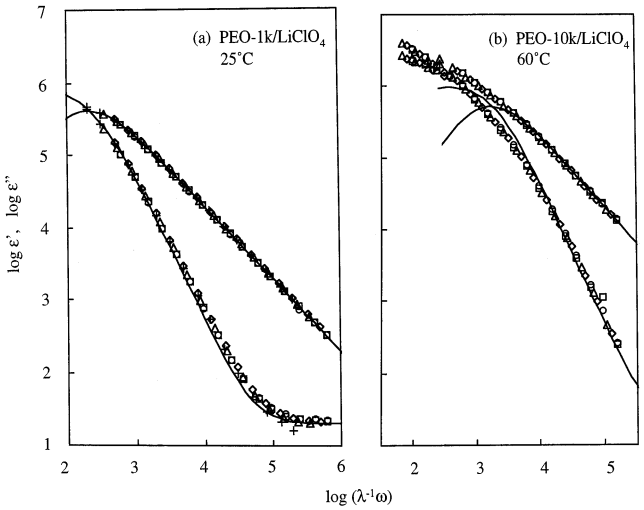

Figure 9. Plots of dynamic dielectric constant ϵ' and dielectric loss ϵ'' against reduced frequency $\lambda^{-1}\omega$ for (a) the PEO-1K/$LiClO_4$ system at 25 °C and (b) the PEO-10K/$LiClO_4$ system at 60 °C. Symbols are the same as those in Figure 8. The solid curves denote the fitting with the Macdonald theory for the data in the quiescent state at equilibrium. The dielectric constant of the medium (PEO) utilized in the fitting was $\epsilon_m'(0) = 20$. For further details, see Appendixes A and B.

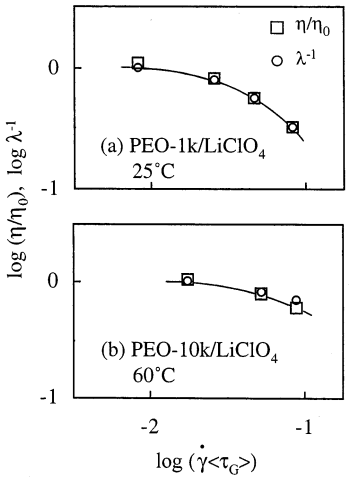

Figure 10. Comparison of the normalized non-Newtonian viscosity η/η_0 and the λ^{-1} factor representing shear-induced acceleration of ion motion for (a) PEO-1K/$LiClO_4$ at 25 °C and (b) PEO-10K/$LiClO_4$ at 60 °C. η/η_0 and λ^{-1} are plotted against reduced shear rate $\dot{\gamma}\langle\tau_G\rangle$.

axis was properly accounted for in the calculation of theoretical $\epsilon'(\omega)$ and $\epsilon''(\omega)$; cf. Appendix B. The solid curves in Figure 9 are the best fits of the Macdonald theory under this assumption through the data in the quiescent state. The parameters obtained from the fitting are

$$\mu = 1.0 \times 10^{-8}\ \mathrm{m^2\ V^{-1}\ s^{-1}} \text{ and } n = 9.6 \times 10^{22}\ \mathrm{m^{-3}}$$
for the PEO-1K/$LiClO_4$ system at 25 °C (4)

and

$$\mu = 6.0 \times 10^{-8}\ \mathrm{m^2\ V^{-1}\ s^{-1}} \text{ and } n = 2.7 \times 10^{23}\ \mathrm{m^{-3}}$$
for the PEO-10K/$LiClO_4$ system at 60 °C (5)

The deviation from the Macdonald curve seen at low frequencies in Figure 9b probably results from an extra slow dispersion due to thin capacitor layers formed at the surface of the electrodes, as found for similar polymer/salt mixtures.[1,14,15] Such layers do not severely affect the quantitative applicability of the Macdonald theory at high frequencies.

The μ values (eqs 4 and 5) obtained from the fitting under the above assumption are regarded to be the mobility averaged for the anion and cation in the PEO-1K/$LiClO_4$ and PEO-10K/$LiClO_4$ systems in the quiescent state at equilibrium. Under steady shear, the mobility increases from these values by the factor λ shown in Figure 10. In contrast, the n values are not affected by the steady shear (as evidenced from the validity of the superposition after the horizontal shift; cf. Figure 9).

The above fitting results also suggest that the fraction of dissociated ions in our systems is very small. The number density of ions expected if all of the salt was dissociated is $n_{full} = 1.4 \times 10^{27}\ \mathrm{m^{-3}}$ (=2.3 kmol $\mathrm{m^{-3}}$; total salt concentration). The n values obtained from the fitting (eqs 4 and 5) are 4 orders of magnitude smaller, and the dissociation constant of $LiClO_4$ in PEO is thus estimated to be $\cong 10^{-4}$. This is consistent with literature values for the dissociation constant of $LiClO_4$ in PEO.[21] Furthermore, the dissociation constant obtained here is similar in magnitude to that obtained for $LiPF_6$/PEO[19] and $LiClO_4$/poly(propylene glycol)[14,15] systems.

Finally, we examine the correlation between the dielectric and rheological behavior under steady shear. Figure 10 shows the dependence of two nondimensional parameters on the reduced shear rate: (1) $\lambda^{-1}(\dot{\gamma})$, the reciprocal of the fractional increase in the ion mobility caused by steady shear at the rate $\dot{\gamma}$, and (2) the $\eta(\dot{\gamma})/\eta_0$ ratio, the fractional decrease in the steady-state viscosity caused by the shear (cf. Figure 7). For both the PEO-1K/$LiClO_4$ system at 25 °C (Figure 10a) and the PEO-10K/$LiClO_4$ system at 60 °C (Figure 10b), the $\eta(\dot{\gamma})/\eta_0$ ratio is in quantitative agreement with the $\lambda^{-1}(\dot{\gamma})$ factor. It should also be noted that both $\eta(\dot{\gamma})/\eta_0$ and λ^{-1} begin to decrease from unity when the reduced shear rate $\dot{\gamma}\langle\tau_G\rangle$ is still smaller than 0.1. This behavior is significantly different from the nonlinear thinning behavior of usual homopolymers (for which η begins to decrease when $\dot{\gamma}\langle\tau_G\rangle$ exceeds unity), confirming the structural origin (disruption of the Li^+-mediated aggregates) of the nonlinearity of the PEO/salt mixtures.

The quantitative agreement between $\eta(\dot{\gamma})/\eta_0$ and $\lambda^{-1}(\dot{\gamma})$ suggests an interesting correlation between the motion of the PEO segments and the motion of the ions. Many studies have indicated that the ions, in particular Li^+, move cooperatively with the PEO segment to which they are bound.[1,7,13] The application of steady shear creates a tension along the PEO chains, leading to the rupture of the Li^+-mediated aggregate. In the ruptured state, the Li^+ ion is bound to the chain less significantly than it is under the quiescent condition, and this leads to the increase in the mobility of both the Li^+ ion and the PEO segments in its vicinity by a common factor, $\lambda(\dot{\gamma})$. This acceleration of the PEO segment motion results in the acceleration of the motion of the PEO chain as a whole so that the viscosity η decreases by the factor $\lambda^{-1}(\dot{\gamma})$. Thus, the observed agreement of the $\eta(\dot{\gamma})/\eta_0$ ratio and $\lambda^{-1}(\dot{\gamma})$ appears to be a natural consequence of the motional cooperativity between the Li^+

ions and the PEO segments to which the ions are bound.

4. Concluding Remarks

The dielectric dispersion of PEO/$LiClO_4$ mixtures under shear flow was examined. The magnitude of shear thinning, observed in the rheological experiments, was well correlated with the flow-induced increase in the electrical conductivity observed in the dielectric experiments. In addition, the increase in the conductivity was found to be mainly due to the increase in the ion mobility under shear flow, as revealed from the superposition of the dielectric data at various shear rates after shifts only along the frequency axis. These results are in harmony with the molecular picture of the motional cooperativity between the PEO segments and the Li^+ ions to which they are bound.

Acknowledgment. This work was conducted under the Batteries for Advanced Transportation Technologies (BATT) Program, supported by the U.S. Department of Energy Office of FreedomCAR and Vehicle Technologies (FCVT).

Appendix A: Macdonald Theory for Electrode Polarization

Macdonald formulated a time-evolution equation for the concentration profiles of ions in a medium containing a dissociated monovalent salt, sandwiched between two flat electrodes used to apply a weak oscillatory electric field.[34] The profiles form standing waves that oscillate at the angular frequency ω of the applied field. The amplitudes of these waves change with the distance from the electrodes. For our PEO/$LiClO_4$ systems sandwiched between stainless steel electrodes, we may safely assume the blocking condition (for which the conduction current due to the ion motion does not flow across the electrodes) and neglect the recombination of the cation (Li^+) and anion (ClO_4^-). For this case, the complex admittance y_P due to the electrode polarization per unit area of the electrode, deduced from the Macdonald theory, can be written in the form

$$y_p = \frac{en(\mu_+ + \mu_-)}{L} + \frac{en}{L}\frac{W_3}{W_1 - W_2} \tag{A1}$$

with

$$W_1 = \frac{(\gamma_+ - 1)(\gamma_- + 1)\vartheta_-(\vartheta_+ - \tanh\vartheta_+)}{\xi_+} - \gamma_+(\gamma_- + 1)\vartheta_+\vartheta_- \tag{A2}$$

$$W_2 = \frac{(\gamma_+ + 1)(\gamma_- - 1)\vartheta_+(\vartheta_- - \tanh\vartheta_-)}{\xi_-} - (\gamma_+ + 1)\gamma_-\vartheta_+\vartheta_- \tag{A3}$$

$$W_3 = (\gamma_- + 1)(\gamma_+\mu_- - \mu_+)\vartheta_- \tanh\vartheta_+ - (\gamma_+ + 1)(\gamma_-\mu_- - \mu_+)\vartheta_+ \tanh\vartheta_- \tag{A4}$$

Here, n is the number density of the cations (identical to that of the anions), e is the absolute value of the electron charge ($e = 1.602 \times 10^{-19}$ C), μ_+ and μ_- are the mobilities of the cation and anion, and L is the gap width between the flat electrodes.

The parameters $\xi_\pm$, $\gamma_\pm$, and $\vartheta_\pm$ are given by

$$\xi_\pm = 1 + i\frac{(\mu_+ + \mu_-)Q\omega}{2\mu_+\mu_-} \pm \left(1 - \frac{(\mu_+ + \mu_-)^2Q^2\omega^2}{4\mu_+^2\mu_-^2}\right)^{1/2} \quad \text{with} \quad i = \sqrt{-1} \tag{A5}$$

$$\gamma_\pm = 1 + i\frac{Q\omega}{\mu_+} - \xi_\pm \tag{A6}$$

$$\vartheta_\pm = \frac{M_\vartheta}{\sqrt{2}}\xi_\pm^{1/2} \tag{A7}$$

with

$$M_\vartheta = \left(\frac{e^2n}{2\epsilon_{vac}\epsilon_m'(0)k_BT}\right)^{1/2}L \quad \text{and} \quad Q = \frac{\epsilon_{vac}\epsilon_m'(0)}{en} \tag{A8}$$

Here, ϵ_{vac} is the dielectric permittivity of a vacuum ($\epsilon_{vac} = 8.854 \times 10^{-12}$ F m^{-1}), k_B is the Boltzmann constant ($k_B = 1.381 \times 10^{-23}$ J K^{-1}), T is the absolute temperature, and $\epsilon_m'(0)$ is the relative dielectric constant of the medium (PEO) at zero frequency. Since PEO chains have only type B dipoles,[40] they exhibit no dielectric loss at the angular frequencies ω of our interest ($\omega < 10^6$ s^{-1}). For this reason, the complex dielectric constant of the medium at a frequency ω, which is included in the general expressions of M_ϑ and Q, has been replaced by $\epsilon_m'(0)$ in eq A8.

The dielectric constant $\epsilon'(\omega)$ and dielectric loss $\epsilon''(\omega)$ (relative to a vacuum) measured for the PEO/$LiClO_4$ system are related to the imaginary and real parts of the complex admittance y_P per unit area:

$$\epsilon'(\omega) = \epsilon_m'(0) + \frac{L}{\omega\epsilon_{vac}}\,\mathrm{Im}\{y_p(\omega)\}, \qquad \epsilon''(\omega) = \frac{L}{\omega\epsilon_{vac}}\,\mathrm{Re}\{y_p(\omega)\} \tag{A9}$$

Note that ϵ' and ϵ'' *at low* ω calculated from eq A9 increase with decreasing L and are not the simple material properties independent of L. At sufficiently high ω, this L dependence vanishes and ϵ' and ϵ'' coincide with ϵ' and ϵ'' of the material itself. At such high ω, eq A9 gives $\epsilon'(\omega) = \epsilon_m'(0)$ and $\epsilon''(\omega) = en(\mu_+ + \mu_-)/\epsilon_{vac}\omega$.

We may estimate the mobilities μ_+ and μ_- as well as the number density n of the ions by fitting the experimental ϵ' and ϵ'' data with eqs A1−A9 modified for our cone−plate-type electrodes (cf. Appendix B). The results of the fitting are shown in Figure 9.

In addition to the estimation of the μ_+, μ_-, and n values, the Macdonald theory offers an easy method for distinguishing two effects of shear on the ionic conductivity. The conductivity $\sigma = en(\mu_+ + \mu_-)$ becomes larger under the shear either through an increase of the ion number density n or through an increase of the mobilities μ_+ and μ_-. However, these two types of increases result in qualitatively different changes in the shape of the dispersion curves (ω dependencies of ϵ' and ϵ''), as demonstrated in Figure 11. (In Figure 11, μ_+ and μ_- are assumed to have the same value μ for simplicity.)

For the case where μ increases by a factor of λ but n remains the same under the shear, the dispersion curve plotted in the double logarithmic scale shifts horizontally toward the high-ω side by the same factor; see the top two panels in Figure 11. Thus, the ϵ' and ϵ'' data

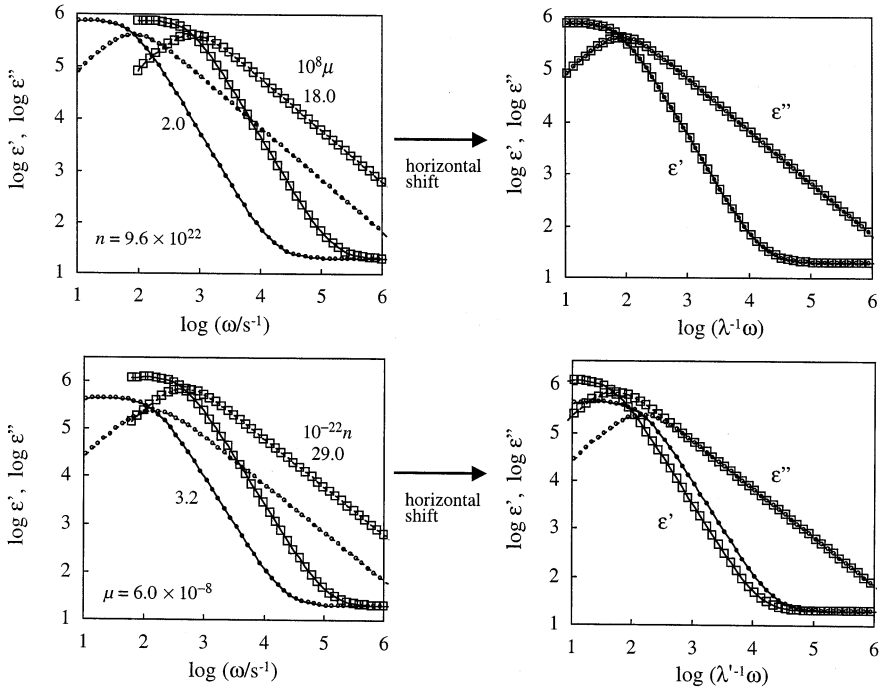

Figure 11. Dielectric dispersion curves calculated from Macdonald theory ($L = 1$ mm, $\mu_+ = \mu_- = \mu$, $\epsilon_m'(0) = 20$, $T = 298$ K). The top left panel shows the curves for two systems having the same ion number density ($n = 9.6 \times 10^{22}$ m^{-3}) but different ion mobilities ($10^{-8}\mu$/m^2 V^{-1} s^{-1} = 2.0 and 18.0). The high-μ curve shifted horizontally by a factor of $\lambda^{-1} = 1/9$ (mobility ratio) is superposed on the low-μ curve, as shown in the top right panel. The bottom left panel shows the curves for two systems having the same μ value (6.0×10^{-8} m^2 V^{-1} s^{-1}) but different n values ($10^{-22}n$/m^{-3} = 3.2 and 29.0). For this case, the horizontal shift of the high-n curve by a factor of $(\lambda')^{-1}$ (ratio of ion number densities) does not achieve the superposition; see the bottom right panel.

horizontally shifted by the factor λ^{-1} (i.e., those plotted against a reduced frequency, $\lambda^{-1}\omega$) are collapsed onto a master curve irrespective of the μ values.

For the other case where n increases by a factor of λ' but μ remains the same under the shear, the dispersion curve around the peak of ϵ'' shifts diagonally toward the high-ω and high-ϵ'' side and the horizontal shift of the ϵ' and ϵ'' data does not give the master curve; see the bottom two panels in Figure 11.

This difference between the two cases of the increases of μ and n, noted not only for the parallel-plate-type electrodes but also for the cone-and-plate-type electrodes (utilized in our experiments), allows us to examine a mechanism of the flow-induced enhancement of the ionic conduction. Indeed, the enhancement observed for the PEO/$LiClO_4$ systems is attributed to the increase of μ, as explained for Figure 9.

Appendix B: Application of Macdonald Theory for Cone−Plate Electrodes

As shown in Figure 1, the electrodes used in our experiments were of the cone-and-plate type (to achieve the uniform shear field between the electrodes). Thus, the gap width between the electrodes, L, changes with radial coordinate r:

$$L = r_c\theta = 0.209 \text{ mm} \quad \text{for} \quad r < r_c \tag{B1}$$

and

$$L = r\theta \quad \text{for} \quad r_c < r < r_0 \tag{B2}$$

Here r_c (=3.6 mm) is the radius of the flattened head area of the cone electrode, r_0 (=13.6 mm) is the radius of the cone electrode, and θ (=0.058 rad) is the cone angle. In our application of the Macdonald theory to the dielectric data, we subdivided the whole area of the cone electrode into six coaxial sections: the first section is in a range of $r < r_c$ and has $L_1 = r_c\theta$ (eq B1), and the remaining five sections are in the range of $r_c + (j-2)\Delta r < r < r_c + (j-1)\Delta r$ ($j = 2-6$, $\Delta r = (r_0 - r_c)/5$) and have an average gap width $L_j = \{r_c + (j - 3/2)\Delta r\}\theta$. Approximating that the jth section of the cone electrode is parallel to the plate electrode and has a constant gap width L_j, we evaluated a vacant capacitance C_{0j} for this section as

$$C_{01} = \frac{\epsilon_{vac}}{L_1}\pi r_c^2,$$

$$C_{0j} = \frac{\epsilon_{vac}}{L_j}[\pi\{r_c + (j-1)\Delta r\}^2 - \pi\{r_c + (j-2)\Delta r\}^2] \quad (j = 2-6) \tag{B3}$$

From these C_{0j} values, a relative contribution ϕ_j of the jth section to the total capacitance of the cell was obtained as $\phi_j = C_{0j}/\sum_{k=1-6}C_{0k}$. The complex dielectric constant $\epsilon^* = \epsilon' - i\epsilon''$ ($i = \sqrt{-1}$) for our rheodielectric cell was then given by

$$\epsilon^* = \sum_{j=1}^{6}\phi_j\epsilon_{M,j}^* \tag{B4}$$

where $\epsilon_{M,j}^*$ is the complex dielectric constant calculated from the Macdonald theory (eqs A1−A9) for the gap width L_j. Changes in this ϵ^* with the changes in n and μ are essentially the same as the changes in $\epsilon_{M,j}^*$ explained in Appendix A. Thus, the change in μ alone results in the horizontal shift of the ϵ^* curve, while the chain in n alone leads to the diagonal shift.

The complex dielectric constant can thus be computed if the parameters μ, n, and $\epsilon_m'(0)$ are known. We adjusted these parameters to match the theory and experiment, and the results of this matching procedure are shown in Figure 9, parts a and b. The value of $\epsilon_m'(0)$ used to obtain the fit was 20 in both cases, while μ and n are given in eqs 4 and 5.

References and Notes

(1) Armand, M. *Solid State Ionics* **1983**, *9*, 745.
(2) Gray, F. M. *Polymer Electrolytes*; Royal Society of Chemistry: Cambridge, 1997.
(3) Watanabe, M.; Endo, T.; Nishimoto, A.; Miura, K.; Yanagida, M. *J. Power Sources* **1999**, *81*, 786.
(4) Fenton, D. E.; Parker, J. M.; Wright, P. V. *Polymer* **1973**, *14*, 589.
(5) Cowie, J. M. G.; Sadaghianizadeh, K. *Solid State Ionics* **1990**, *42*, 243.
(6) Fauteux, D.; Robitaille, C. *J. Electrochem. Soc.* **1986**, *133*, 315.
(7) Watanabe, M.; Ogata, N. *Br. Polym. J.* **1988**, *20*, 181.
(8) Watanabe, M.; Sanui, K.; Ogata, N.; Kobayashi, T.; Ohtaki, Z. *J. Appl. Phys.* **1985**, *57*, 123.
(9) Bridges, C.; Chadwick, A. V.; Worboys, M. R. *Br. Polym. J.* **1988**, *20*, 207.
(10) Kim, D.; Ryoo, B.; Park, J.; Maeng, K.; Hwang, T. *Polym. J.* **1992**, *24*, 519.
(11) Kakihana, M.; Schantz, S.; Torell, L. M.; Stevens, J. R. *Solid State Ionics* **1990**, *40/41*, 641.
(12) Mitani, K.; Adachi, K *J. Polym. Sci., Part B: Polym. Phys.* **1995**, *33*, 937.
(13) Mitani, K.; Adachi, K *J. Polym. Sci., Part B: Polym. Phys.* **1995**, *33*, 947.
(14) Sakurai, T. Electrode Polarization in Polymers with Ionic Conduction. M.S. Dissertation, Graduate School of Science, Osaka University, 1995.
(15) Sakurai, T. *Rheol. Prepr.-III Jpn.* **1995**, *13*, 37. Uemura, S.; Sakurai, T. Private communication.
(16) Wright, P. V. *Br. Polym. J.* **1975**, *7*, 319.
(17) Borodin, O.; Smith, G. D. *Macromolecules* **1998**, *31*, 8396.
(18) Halley, J. W.; Duan, Y.; Curtiss, L. A.; Baboul, *J. Chem. Phys.* **1999**, *111*, 3302.
(19) Vachon, C.; Vasco, M.; Perrier, M.; Prud'homme, J. *Macromolecules* **1993**, *26*, 4023
(20) Borodin, O.; Doughlas, R.; Smith, G.; Eyring, E. M.; Petrucci, S. *J. Phys. Chem. B* **2002**, *106*, 2140
(21) Petrucci, S.; Eyring, E. M. *Phys. Chem. Chem. Phys.* **2002**, *4*, 6043
(22) Yano, S. *J. Polym. Sci., Part A-2* **1970**, *8*, 1057.
(23) Kosaki, M.; Ohsima, H.; Ieda, M. *J. Phys. Soc. Jpn.* **1970**, *29*, 1012.
(24) Riande, E.; Saiz, E. *Dipole Moments and Birefringence of Polymers*; Prentice Hall: Englewood Cliffs, NJ, 1992.
(25) Matsumiya, Y.; Watanabe, H.; Inoue, T.; Osaki, K.; Yao M. L. *Macromolecules* **1998**, *31*, 7973.
(26) Watanabe, H.; Sato, T.; Hirose, M.; Osaki, K.; Yao, M. L. *Rheol. Acta* **1998**, *37*, 519.
(27) Watanabe, H.; Sato, T.; Hirose, M.; Osaki, K.; Yao, M. L. *Rheol. Acta* **1999**, *38*, 100.
(28) Watanabe, H.; Sato, T.; Matsumiya, Y.; Inoue, T.; Osaki, K. *J. Soc. Rheol. Jpn.* **1999**, *27*, 121.
(29) Watanabe, H.; Matsumiya, Y.; Kakiuchi, M.; Aoki, Y. *J. Soc. Rheol. Jpn.* **2001**, *29*, 77.
(30) Watanabe, H.; Ishida, S.; Matsumiya, Y. *Macromolecules* **2002**, *35*, 8802.
(31) Watanabe, H.; Matsumiya, Y.; Inoue, T. *J. Phys.: Condens. Matter* **2003**, *15*, S909.
(32) (a) At temperatures well above the glass transition temperature T_g, the WLF-type temperature dependence of the linear viscoealstic moduli G' and G'' of neat amorphous polymers is indistinguishable from the Arrhenius-type dependence.[33] For neat PEO, the melting temperature T_m (40 °C for PEO-1K and 67 °C for PEO-10K and PEO-20K) was much higher than T_g (reported to be between −40 and −115 °C[32c]). For this reason, we observed the Arrhenius-type temperature dependence of G' and G'' of neat PEO at $T > T_m$. This dependence was successfully utilized to make short extrapolation of the G' and G'' data of neat PEO to the temperatures examined in Figures 4 and 5. (b) The dielectric dispersion seen for the neat PEO (at $T > T_m$) is due to motion of ionic impurities causing the electrode polarization. This motion would be coupled (to some extent) with the motion of the PEO segment to exhibit an Arrhenius-type accerelation with increasing temperature. In addition, the concentration of the dissociated impurities should exhibit an Arrhenius-type increase. For these reasons, we observed the Arrhenius-type temperature dependence of ϵ' and ϵ'' of neat PEO at $T > T_m$ (characterized by an activation energy ΔE that agreed, within 30%, with ΔE for the viscoelastic moduli). This dependence was successfully utilized to make short extrapolation of the ϵ' and ϵ'' data of neat PEO to the temperatures examined in Figures 2 and 3. (c) Peyser, P. Glass Transition Temperature of Polymers. In *Polymer Handbook*, 3rd ed.; Brandrup, J., Immergut, E. H., Eds.; Wiley: New York, 1989.
(33) Ferry, J. D. *Viscoelastic Properties of Polymers*, 3rd ed.; Wiley: New York, 1980.
(34) Macdonald, J. R. *Phys. Rev.* **1953**, *92*, 4.
(35) Matsumiya, Y.; Balsara, N. P.; Kerr, J. B.; Inoue, T.; Watanabe, H. Manuscript in preparation.
(36) Watanabe, H. *Prog. Polym. Sci.* **1999**, *24*, 1253.
(37) Hommes, N. J. R. v. E.; Buhl, M.; Schleyer, P. v. R. *J. Organomet. Chem.* **1991**, *409*, 307.
(38) Under fast shear at $\dot{\gamma} > 100\ s^{-1}$, the PEO-20K/$LiClO_4$ system could not stay in the gap between the cone and plate (electrodes) over long times because of its significant elasticity (cf. Figure 4c). Thus, the gradual shear thinning behavior of this system under fast shear could not be tested experimentally, though this behavior is naturally expected.
(39) (a) We estimated the temperature increase due to viscous dissipation using the equations given in ref 39b. The largest effect was obtained for the PEO-1K/$LiClO_4$ system at 25 °C, where we calculated a maximum temperature increase ΔT of 1.0 °C, using the steady-state viscosity $\eta(\dot{\gamma}) = 6.3$ Pa s at $\dot{\gamma} = 1000\ s^{-1}$ and the thermal conductivity of PEO (0.2 W/m K[39c]). This small ΔT is not responsible for the significant decrease of $\eta(\dot{\gamma})$ under fast shear (Figure 7). (b) Bird, R. B.; Stewart, W. E.; Lightfoot, W. N. *Transport Phenomena*; Wiley: New York, 1960. (c) Song, L.; Chen, Y.; Evans, J. W. *J. Electrochem. Soc.* **1997**, *144*, 3797.
(40) Stockmayer, W. H. *Pure Appl. Chem.* **1967**, *15*, 539.

MA0304473